Journal of Rock Mechanics and Geotechnical Engineering 8 (2016) 1–15

Contents lists available at ScienceDirect

Journal of Rock Mechanics and Geotechnical Engineering

journal homepage: www.rockgeotech.org

Full length article

The influence of microwave irradiation on rocks for microwave-assisted underground excavation

Ferri Hassani*, Pejman M. Nekoovaght, Nima Gharib

Department of Mining and Material Engineering, McGill University, Montreal, Canada

ARTICLE INFO

Article history:
Received 14 September 2015
Received in revised form
30 September 2015
Accepted 14 October 2015
Available online 8 December 2015

Keywords:
Microwaves
Crack density
Microwave-assisted tunnel boring
Rock breakage

ABSTRACT

Demand is growing for explosive-free rock breakage systems for civil and mining engineering, and space industry applications. This paper highlights the work being undertaken in the Geomechanics Laboratory of McGill University to make a real application of microwave-assisted mechanical rock breakage to full-face tunneling machines and drilling. Comprehensive laboratory tests investigated the effect of microwave radiation on temperature profiles and strength reduction in hard rocks (norite, granite, and basalt) for a range of exposure times and microwave power levels. The heating rate on the surface of the rock specimens linearly decreased with distance between the sample and the microwave antenna, regardless of microwave power level and exposure time. Tensile and uniaxial compressive strengths were reduced with increasing exposure time and power level. Scanning electron micrographs (SEMs) highlighted fracture development in treated basalt. It was concluded that the microwave power level has a strong positive influence on the amount of heat damage induced to the rock surface. Numerical simulations of electric field intensity and wave propagation conducted with COMSOL Multiphysics® software generated temperature profiles that were in close agreement with experimental results.

1. Introduction

Since World War II, many devices that use microwaves have been designed and manufactured (Osepchuk, 1984). Microwave frequencies are broadly reserved for telecommunications (Gwarek and Celuch-Marcysiak, 2004). The industrial, scientific and medical (ISM) sector uses frequencies of 915 MHz and 245 GHz (Gwarek and Celuch-Marcysiak, 2004; Brodie, 2011). The concept of using microwave energy to generate heat for rock drilling was briefly examined in the 1960s (Maurer, 1968), but due to technical issues at the time, it was not deemed economical and was not further investigated. Microwave applications have primarily been investigated for the mineral processing industry to reduce energy requirements during comminution of ores and increase the liberation of valuable mineral particles for enhanced separation (Fitzgibbon and Veasey, 1990; Harrison, 1997; Kingman and Rowson, 1998; Kingman et al., 1998, 2004; Whittle et al., 2003; Scott, 2006).

Among the many rock breakage methods available (Hassani, 2010), mechanical rock breakage has been proven to be the most economical and hence the most commonly used one. As current technologies advance and raw materials become more scarce and valuable, the importance of developing novel rock breakage methods increases. The microwave rock breakage technique was introduced in the 1960s (Gray, 1965; Maurer, 1968). Since then, microwaves have been widely and increasingly used in food- (Metaxas and Meredith, 1983; Meredith, 1998), and health-related industries (Saxena, 2009) and for mineral processing (Walkiewicz et al., 1991; Kingman et al., 2004; Scott, 2006).

During hard rock breakage (i.e. the separation of a piece of rock from its parent deposit) in mining and civil applications, the performance of mechanical equipment such as tunnel boring machines (TBMs) is limited by high levels of bit wear and maintenance. Preconditioning to weaken natural rock prior to mechanical breakage is one approach to lower bit wear, maintenance requirements, and costs (Nekoovaght and Hassani, 2014; Nekoovaght et al., 2014a, b, c, 2015; Hassani and Nekoovaght, 2011, 2012; Hassani et al., 2008, 2011, 2012). Preconditioning methods apply heat either directly or indirectly. For example, flame torch-assisted TBMs (Lauriello and Fritsch, 1974; Resource Technology Inc, 1984) have been deemed economical in terms of equipment, but their feasibility is limited by high fuel consumption and because they emit fumes. Preconditioning with microwave energy offers several advantages over the flame torch method: it does not increase fuel consumption (electricity source is available on the machine) or

* Corresponding author. Tel.: +1 514-398-8060.
E-mail addresses: ferri.hassani@mcgill.ca, ferrihassani@hotmail.com (F. Hassani).

Peer review under responsibility of Institute of Rock and Soil Mechanics, Chinese Academy of Sciences.
1674-7755
http://dx.doi.org/10.1016/j.jrmge.2015.10.004

produce emissions, and is easy to be controlled (quick power on and off).

1.1. Microwave systems

The specifications of a given microwave system depend upon the intended application. Generally, commercial microwave ovens use low power (up to 3 kW) and consist only of a magnetron, a short waveguide, and a closed metallic cavity (oven). Industrial microwave systems use higher power levels (3–200 kW) and comprise the magnetron, isolator, power meter waveguides, tuner, cavity, and power generator. The magnetron generates the microwave energy, which is then transmitted to the cavity by the waveguides, which are long, hollow rods made of a dielectric material to reflect all microwaves. The physical dimensions of the magnetron, isolator, waveguide, and tuner are directly related to the microwave frequency. A microwave with a frequency of 2.45 GHz has a wavelength of 12.2 cm, and travels through a standard WR340 waveguide with dimensions of 9 cm × 4.5 cm.

A single-mode cavity (only one mode of energy is excited within it) has the same dimensions as the waveguide that is used for a given frequency. A multimode cavity is a closed metallic box with dimensions several times the wavelength, resulting in a chaotic energy distribution once microwaves enter the cavity. Although one mineral can also be heated by conduction from adjacent minerals in a multimode cavity, the power density created is 10–15 times greater than that in a single-mode cavity (Kingman et al., 1998, 2004).

1.2. Mineral and rock responses to microwave treatment

The amount of heat produced in a given rock by microwave treatment depends on the microwave power level and exposure time, and the mineral and chemical compositions of the rock. Some minerals absorb (e.g. pyrite) and some are transparent to microwaves (e.g. calcite) (Chen et al., 1984; Walkiewicz et al., 1991). Differential volumetric expansion of mineral constituents of rock during heating creates stress along grain boundaries, and causes inter- and trans-granular cracks, which can weaken the rock. For example, the Bond Work Index was up to 90% lower in a massive Norwegian ilmenite ore after microwave treatment (Kingman et al., 1998). Exposing a simulated pyrite-hosted calcite sample to microwave radiation reduced uniaxial compressive strength (UCS) and tensile strength (Whittle et al., 2003; Wang et al., 2005).

The electromagnetic spectrum is comprised of different sections according to its range of frequencies. Within these range of frequencies, microwaves cover the range from 0.3 GHz to 3 GHz. Electromagnetic waves consist of an electric and a magnetic wave traveling perpendicular to each other. Electromagnetic waves transport energy with the speed of light within space. Microwaves as part of the electromagnetic spectrum decay as they penetrate into a dielectric material, at a rate that depends on the electrical and physical characteristics of that material. The penetration depth, also known as the skin depth in metals, is the depth from the surface at which waves attenuate to $1/e$ ($e = 2.718$ as the Euler's number) of their initial power value. The penetration depth depends on the frequency of the electromagnetic waves and the electrical permittivity of the material (Metaxas and Meredith, 1983). For dielectric materials such as rocks (Schön, 2004), which have a loss factor that is much smaller than the dielectric constant, the penetration depth of microwaves is calculated as

$$z = \frac{\lambda_0\sqrt{\varepsilon'}}{2\pi\varepsilon''} \tag{1}$$

where z is the penetration depth (m), λ_0 is the wavelength of the appropriate frequency (m), ε' is the dielectric constant of the material, and ε'' is the loss factor of the material.

The volumetric energy absorbed by a dielectric in an electromagnetic field (P) is calculated by (Saxena, 2009):

$$P = 2\pi f \varepsilon_0 \varepsilon'' E^2 \tag{2}$$

where f is the frequency (Hz), ε_0 is the permittivity of free space (8.85×10^{-12} F/m), and E^2 is the root mean square of the electric field strength.

The energy absorbed by the material causes the temperature of the material to increase (Metaxas and Meredith, 1983). According to thermo-dynamic law, the amount of energy required to increase the temperature of a material to a given amount is calculated by (Griffiths, 1999):

$$P = \rho C_p \frac{\Delta T}{\Delta t} \tag{3}$$

where ρ is the density of the material (kg/m^3); C_p is the specific heat capacity of the material (J/(kg K)); ΔT is the temperature difference of the material (K), $\Delta T = T_2 - T_1$; and Δt is the time difference from its initial value (s), $\Delta t = t_2 - t_1$.

The electric field and power density of the electromagnetic energy decrease exponentially within the material that is exposed to microwaves from an open waveguide (Metaxas and Meredith, 1983):

$$P(z) = P_0 e^{-z/z_0} \tag{4}$$

where $P(z)$ is the power density at depth z, P_0 is the incident power density, and z_0 is the depth at which the power density magnitude decays to $1/e$ of its value at the surface.

The current study is a part of a project at the Geomechanics Laboratory at McGill University that evaluates the influence of microwave radiation on the surface of hard rock. The goal of the project is to develop new rock breakage techniques for underground excavation applications, where microwave energy is radiated from a pyramidal open-ended horn antenna onto the rock surface in underground openings.

1.3. Rock breakage

Disc cutters are commonly used on continuous TBMs in hard rock excavations, where they roll on the surface of rock and penetrate into it by applying a large thrust perpendicular to the surface of the rock. The penetration of disc cutters depends on machine parameters, and the mechanical properties of the rock mass. The thrust force and rolling force are adjusted and defined such that they exceed the strength of the rock mass. The life of the cutter and the penetration per revolution (P_{Rev}) can be calculated from Eqs. (5)–(7) (Wijk, 1992):

$$L = \sum dw^3 \frac{\cot\theta}{F_n\sqrt{\sigma_{UCS}\sigma_{PLT}}(CAI)^2} \tag{5}$$

$$P_{Rev} = 624\frac{F_n}{\sigma_{Bt}} \tag{6}$$

$$P_{Rev} = 3940\frac{F_n}{\sigma_{UCS}} \tag{7}$$

where L is the life index of the cutter wear (hr), d is the cutter diameter (m), w is the width of the cutter edge (m), θ is one half of

the disc cutter's tip angle (°), F_n is the thrust force applied by the disc cutter (N) (the normal force in response to the applied thrust), σ_{UCS} is the UCS of rock (MPa), σ_{PLT} is the point load index of the rock, *CAI* is the Cerchar abrasivity index of the rock's surface, and σ_{Bt} is the Brazilian tensile strength (BTS) of rock (MPa).

Hypothetically, less thrust is needed to break the surface of a rock pre-weakened by microwave treatment. In other words, the penetration rate can be increased on the pre-weakened rock surface with the same original thrust. The concept is to implement microwave antennas on the cutter head of a continuous TBM such that the surface of the tunnel face is irradiated by microwave energy prior to being cut (Fig. 1).

2. Methods

2.1. Multimode cavity experiments

Temperature profiles, BTS, and UCS were measured after microwave treatment in a multimode cavity at a frequency of 2.45 GHz for four rock types: mafic norite from the Sudbury igneous complex basin (2.8 g/cm^3), granite from Vermont region (2.65 g/cm^3), basalt from Chifeng, China (basalt #1, 2.89 g/cm^3), and basalt from California (basalt #2, 2.78 g/cm^3). The norite and basalt #2 samples were collected from mines that used drilling and blasting, which caused several faults and fractures within the boulders to be cored. Mafic norite has large grains and contains a significant amount of sulfide and mafic minerals, which are considered good absorbers of microwave radiation (Chen et al., 1984): they heat and expand relatively quickly. Granite contains more than 70% silica minerals, which are transparent to microwave energy and do not absorb microwaves to generate heat (Chen et al., 1984). Basalt has fine grains and low porosity.

Cores from rock samples were 50 mm in diameter. Discs for BTS testing were 25 mm high and cylindrical cores used for UCS testing were 100 mm high. The ends of cores were cut and polished according to the International Society for Rock Mechanics suggested techniques and ASTM standards D7012-04 and D3967-05 (ASTM International, 2004, 2005).

Triplicate dry specimens were randomly assigned to treatment at three microwave power levels (1.2 kW, 3 kW, and 5 kW) and four exposure times (0 s, 10 s, 65 s, and 120 s). The temperature at center of the top surface of each specimen was measured immediately after microwave treatment with an infrared gun, which calculates an average temperature from 18 points over an area of 700 mm^2 on the surface of the specimen.

Ultra-sound probes were used to detect deficiencies inside cylindrical rock specimens once immediately after being treated with microwave radiation and once again after being cooled down to the ambient temperature. The results obtained from both ultra-sound tests demonstrated that damage caused by microwave treatment does not change if specimens are left to be cooled down to the ambient temperature; therefore, all experiments were conducted on specimens at room temperature. Once specimens were cooled to ambient temperature, they were subjected to two tests. The BTS test was conducted on disc-shaped specimens using a mechanical press machine. The UCS test was conducted on cylinders with a servo-controlled press machine. The specimens for BTS as well as UCS tests were prepared according to the standard procedure introduced in ASTM International (2004, 2005). Results are reported as means of ±1 standard deviation (SD).

A selection of disc-shaped basalt #1 specimens was examined under a scanning electron microscope (SEM) to study microfractures that occurred after microwave treatment.

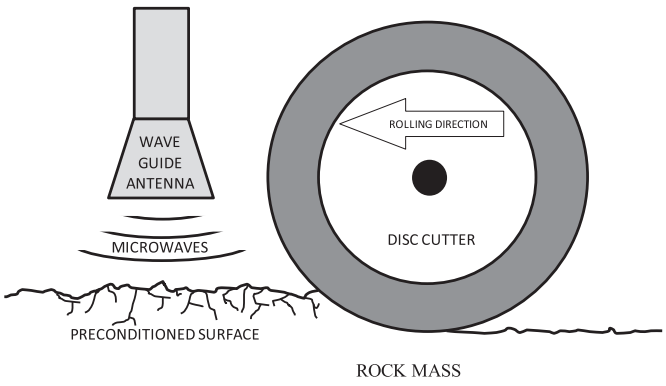

Fig. 1. Schematic of a microwave-assisted disc cutter concept of a continuous TBM.

2.2. Field simulation of basalt preconditioning

To represent field conditions, a custom-made microwave system was designed with variable power up to 3 kW at a constant frequency of 2.45 GHz (Fig. 2). Regardless of the material type, some energy is always reflected back to the magnetron (also known as the microwave generator). This energy was measured with a power meter installed on the waveguide. A water-cooled isolator is connected to the magnetron to limit energy reflection back to the magnetron. Reflected energy is absorbed by the water circulating within the isolator instead of hitting the magnetron antenna. A three-stub tuner between the magnetron and the closed multimode cavity facilitates adjusting the optimum transmission of energy in the waveguide. A rectangular waveguide feeds the microwave energy to the closed 60 cm × 60 cm × 60 cm cavity and spreads the energy throughout a pyramid-shaped horn antenna (aperture 15 cm × 10 cm (width × length)) inside the cavity.

To measure the temperature distribution in rock at various distances from the horn antenna, slab-shaped (40 cm × 40 cm × 2 cm (width × length × height)) intrusive basalt specimens were prepared. Blocks of basalt were created by stacking 12 slabs, which were cut perfectly flat, such that the gap between two slabs was no more than 1 mm (Fig. 2). This gap is negligible compared to the 12.2 cm wavelength of the microwaves. Therefore, the loss of energy within the slabs was assumed to be negligible and insufficient air was present in the space to cool the surfaces within the very short exposure time. In essence, this configuration acted as an intact block of rock and made it easy to adjust the distance between the surface of the rock and the antenna. The electrical and physical properties of the basalt tested are listed in Table 1.

To saturate slabs, new slabs of rock were completely submerged in water for at least 72 h, with spaces between each slab to allow water circulate between slabs. To avoid retention of water between the slabs, surface water was wiped off with a wet towel before the slabs were stacked. To measure the water content according to the standard procedure, a smaller specimen was submerged in water in a standard vacuum chamber. The water content was less than 1.5%, indicating that the basalt is not permeable and has extremely low porosity. A water content of 1.5% falls within the experimental error zone.

Basalt blocks were positioned under the horn antenna such that the antenna aperture localized in the middle of the rock surface to emit the energy. The largest dimension of the horn aperture was much smaller than the width of the slab. Therefore, wave propagation was concentrated on the rock surface, rather than randomly propagating in the cavity.

Basalt blocks were exposed to microwaves at 3 kW power for 60 s or 120 s at six distances from the antenna (3.5 cm, 6.5 cm, 9 cm, 12 cm, 15 cm, and 19.5 cm) for wet basalt and three distances from

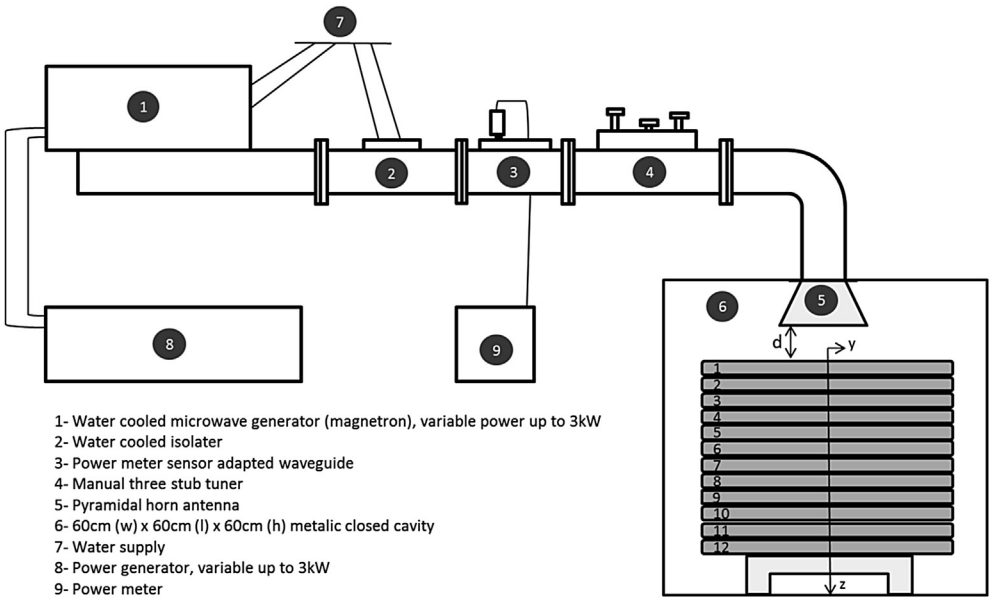

Fig. 2. Schematic view of variable 3 kW power microwave system (Nekoovaght et al., 2014b).

Table 1
Electrical and physical properties of basalt used in the study.

Thermal conductivity, k (W/(m °C))	Electrical conductivity, σ (S/m)	Specific heat capacity, C_p (kJ/(kg K))	Dielectric constant, ε'	Dielectric loss factor, ε''	Loss tangent, tan δ	Electrical resistivity, R (Ω m)	Density, ρ (kg/m^3)	Emissivity, ε
0.6 (Carmichael, 1988)	0.00005 Carmichael, 1988)	1.3702462	8.60975	1.3528	0.1570598	20,000 (Carmichael, 1988)	2870	0.99 (Meredith, 1998)

the antenna (3 cm, 9 cm and 15 cm) for dry basalt. The surface temperature at the middle of each slab was measured with the infrared gun described above immediately after microwave irradiation along the z-axis (Fig. 2), directly in front of the horn antenna. Temperatures were plotted versus the distance from the surface of the rock to the depth along the z-axis. Each trial was conducted three times and the data were reported as mean values.

A 5 cm × 5 cm area was examined in the middle of each slab beneath the horn antenna for macro-crack density (Fig. 3). The surface area was polished with graded sand paper on an automatically turntable and photographed with a 15 megapixel digital camera (Fig. 3). An additional layer was created in Photoshop, where a 9 pt thick red line was drawn on every visible crack. The remaining area was filled with gray. The fraction of the total number of pixels occupied by red permitted calculation of the density of red lines within the total surface area, which is referred to as the macro-crack density. The Griffiths theory (Hoek and Bieniawski, 1965) states that there are pre-existing micro- and macro-cracks within every rock mass. We did not quantify cracks before treatment; however, we assumed the first 0.5% density constitutes pre-existing cracks.

2.3. Two- and three-dimensional models of electric field

Basalt blocks exposed to microwaves have been modeled using COMSOL Multiphysics® software in both two- (2D) and three-dimensional (3D) scenarios. The results obtained from modeling were compared with the equivalent empirical results. The electric

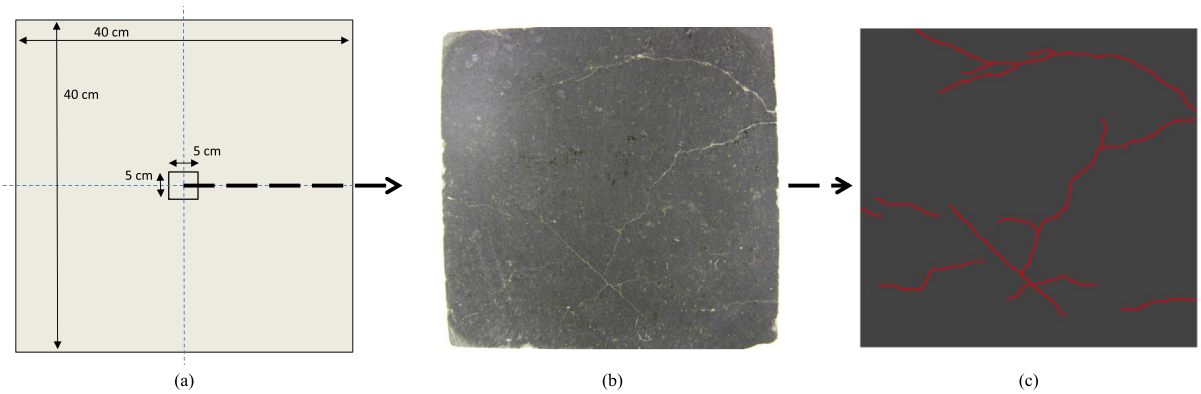

Fig. 3. Schematic of 5 cm × 5 cm square (a) cut out of each 40 cm × 40 cm basalt slab, (b) photograph, and (c) cracks traced in red.

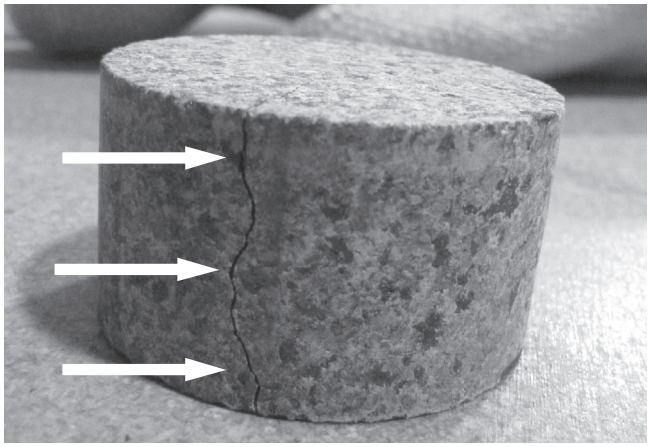

Fig. 4. Norite disc showing crack after microwave treatment for 30 s at 5 kW power.

field is complex enough to be calculated empirically; however, it is easily measured numerically with COMSOL Multiphysics 3D models. The heat dissipation at various depths of the sample exposed to microwave is calculated by modeling electric field inside the cavity.

3. Experimental results and discussion

3.1. Norite temperature profiles, BTS and UCS

Discs of norite cracked in the cross section of the radius after treatment at 3 kW power for 120 s and at 5 kW power for only 30 s (Fig. 4). At 65 s of exposure at 5 kW, the center of the specimen turned red (the first sign that a material will melt). Thus, the higher the power was, the earlier the specimen approached the melting point. This also indicates that the power density absorbed by the rock is much higher at the higher power level. Temperature increased approximately linearly with power level and exposure time.

Untreated norite had a BTS of approximately 15 MPa. A 10 s exposure did not affect BTS at any power level (Fig. 5). Exposure for 65 s and 120 s led to a similar linear decrease in BTS with increasing power level (Fig. 5), which allowed for the use of the 5 kW power without melting the sample and achieving the maximum BTS reduction with a shorter exposure time. At 65 s of exposure, the BTS was reduced by approximately 25%, 35%, and 50% at 1.2 kW, 3 kW, and 5 kW power, respectively.

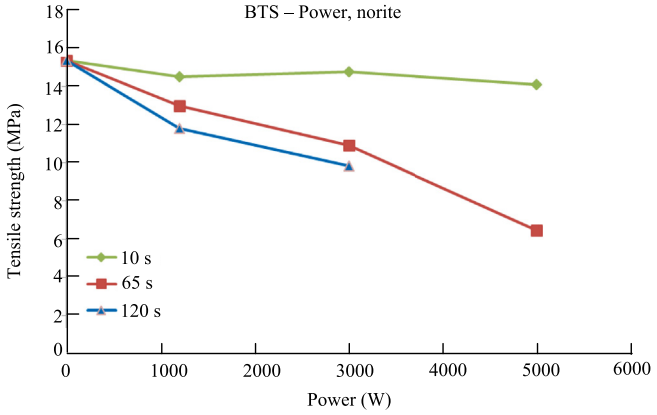

Fig. 5. Norite BTS vs. microwave power level for 10 s, 65 s, and 120 s exposure times.

Unlike BTS, the UCS of untreated norite (200 MPa) did not change after microwave treatment at 1.2 kW and 3 kW power. At 5 kW power, the UCS decreased by more than 25% after 120 s of exposure and cracks began to appear (Fig. 6a). At 65 s, two specimens started to melt in the center at approximately 30 mm from the top and cracked in various parts due to volumetric expansion of solid to liquid stage (Fig. 6b). Since the goal of the study is to keep the rock in its brittle stage, melting is the uppermost limit of the experiment. Melted specimens including the one treated at 5 kW power and 65 s of exposure time are excluded from any experimental tests.

Among the numerous factors involved in determining the penetration rate of a TBM, the BTS, UCS, normal thrust by the machine, and rock surface condition (micro- and macro-fracturing) play a significant role. By using Eqs. (6) and (7), the penetration rate of a TBM was estimated for norite and plotted against the microwave exposure time for three power levels (Fig. 7). The penetration rate of untreated norite was estimated to be 40 mm/rev, whereas at 1.2 kW and 3 kW power after 120 s exposure, the penetration rate increased to only 50 mm/rev and 60 mm/rev, respectively. However, 5 kW of power dramatically increased the penetration rate to 100 mm/rev after 65 s exposure.

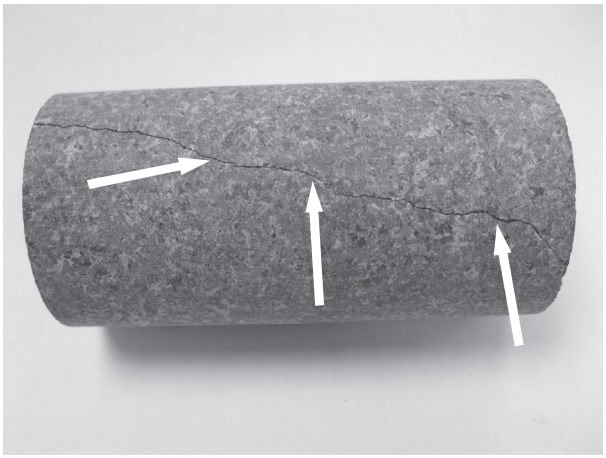

(a)

(b)

Fig. 6. Norite cylinder cracked after (a) 120 s and (b) 65 s after microwave treatment at 5 kW power.

In addition to improving the TBM efficiency and advancement rate, microwave treatment could improve the efficiency of rock comminution and mineral processing. Since the rock mass in front of the cutter head of the TBM is irradiated with microwave energy, the pieces of rock chipped out of the face are also weakened by microwave energy. The pieces conveyed out of the tunnel are already considered as treated rocks prior to reaching the comminution or processing plant.

3.2. Granite temperature profiles, BTS and UCS

The low absorption ability of the granite caused the generation of numerous sparks during treatment; the microwave behaved as if there was no load in the microwave cavity. Hence, although there was an approximately linear increase in surface temperature with power level, the slope of the line was gentle. The temperature of granite discs increased more rapidly and reached a higher value (state maximum temperature for discs here) than cylinders because of their smaller volume. After 120 s of exposure at 5 kW power, cylindrical specimens only reached approximately 200 °C, a temperature that would not be sufficient to induce major physical changes.

Microwave treatment at 1.2 kW power did not affect the BTS of granite; however, at 65 s of exposure time the specimen became stronger, since at low power, rock's temperature rose slowly and gradually, hence, uniformly. But 3 kW and 5 kW of power reduced the BTS more than 20% (Fig. 8). Not surprisingly, the BTS of the granite at all power levels and exposure times did not change from the initial value of 176 MPa.

3.3. Basalt #1 temperature profiles, BTS and UCS

Disc-shaped basalt #1 specimens treated for more than 90 s at 1.2 kW, 35 s at 3 kW or 20 s at 5 kW began to spall off the surface and finally to burst (Fig. 9), as was seen by Gray (1965) and Wilkinson and Tester (1993). The temperature increase was approximately linear with increasing exposure time and power level for both cylinders and discs (data not shown).

The BTS of untreated basalt #1 was approximately 13 MPa (Fig. 10). The 1.2 kW power level had no effect on the BTS, nor did 10 s exposure time at any power level. At 3 kW power, the specimens burst at 35 s. Therefore, an additional exposure time of 20 s was added; BTS was reduced by more than 40%.

At all three power levels, the UCS of basalt #1 remained unchanged from 231 MPa for the 120 s exposure period (data not shown). At 3 kW power and 120 s exposure, the samples burst (Fig. 11), as the samples treated at 5 kW power for 45 s did.

The surface of untreated basalt #1 appeared to be free of fractures at ×50 magnification under the SEM (Fig. 12a), but a few micro-fractures were observed at ×200 magnification (Fig. 12b).

Exposing the basalt to microwave radiation at 3 kW power for a few seconds increased the density of the micro-fractures, visible even at ×50 magnification (Fig. 13a).

3.4. Basalt #2 temperature profiles, BTS and UCS

Basalt #2 discs could not be exposed to microwave energy for more than 35 s at 5 kW power without melting from the center.

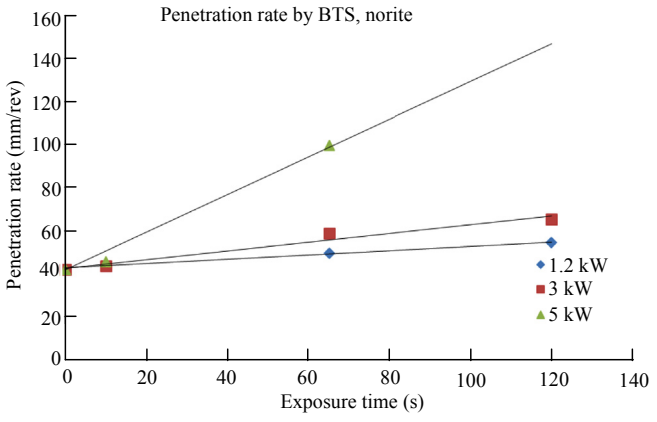

Fig. 7. Estimated penetration rate of a TBM into norite vs. microwave treatment exposure time for three power levels.

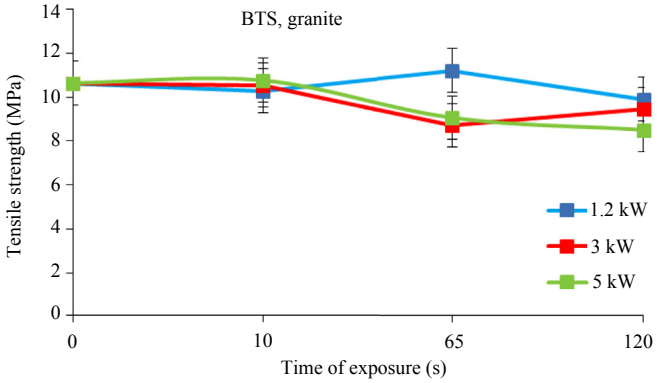

Fig. 8. Granite BTS vs. exposure time.

Fig. 9. Basalt #1 showing surface spalling after microwave treatment for 35 s at 3 kW power.

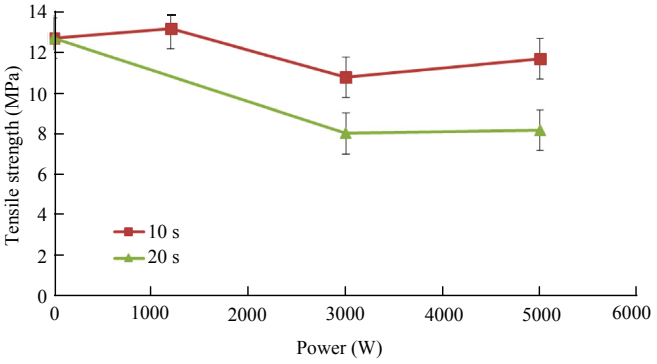

Fig. 10. Basalt #1 BTS vs. microwave power level at 10 s and 20 s exposure times.

Fig. 11. Basalt #1 cylinders burst after microwave treatment for 120 s at 3 kW power.

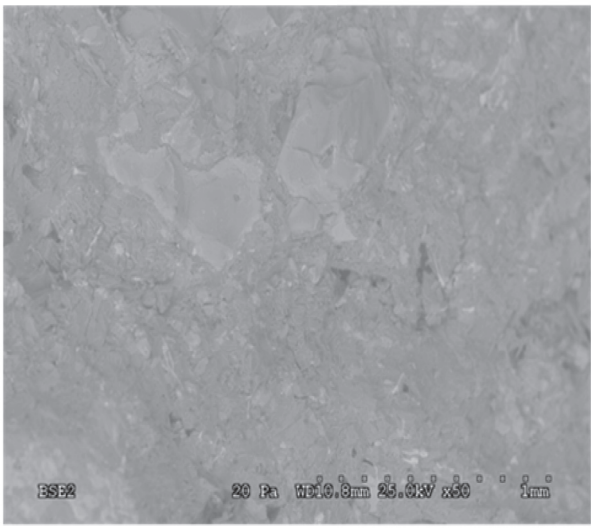

(a)

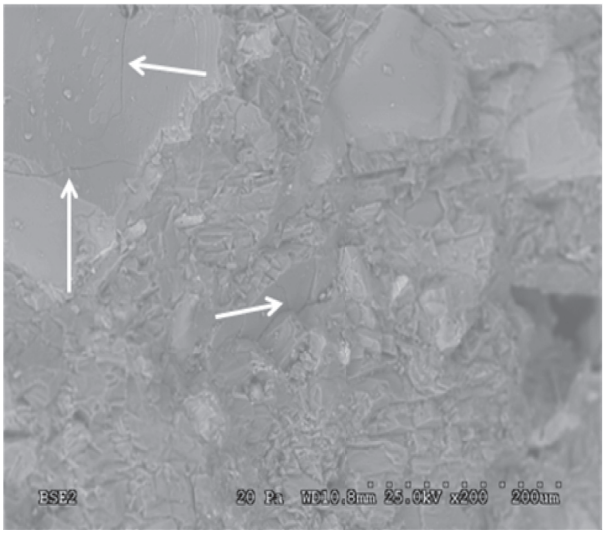

(b)

Fig. 12. Untreated basalt #1 SEM images at (a) ×50 and (b) ×200 magnifications.

Therefore, a 25 s exposure period was tested and discs cracked. Discs treated for 65 s at 3 kW cracked but started to melt at 120 s at the same power (Fig. 14).

The temperature of basalt #2 specimens linearly increased at a much greater rate than other rock types as the power level increased. For instance, disc-shaped specimens treated for 120 s at 1.2 kW, 65 s at 3 kW, and 35 s at 5 kW reached the same temperature (data not shown). Similarly, cylinders were not exposed for more than 65 s at 5 kW in order to avoid the risk of melting.

Untreated basalt #2 had a BTS of 11 MPa. Microwave treatment at 1.2 kW power and 120 s reduced BTS by 20%–30% (data not shown). The UCS of untreated basalt #2 was approximately 140 MPa. Power levels of 1.2 kW and 3 kW had little effect on the UCS at any exposure time, whereas 5 kW power reduced the UCS by approximately 30% after 65 s (Fig. 15). Although exposure of 25 s at 5 kW power showed a slight reduction in the UCS value, the result was not conclusive due to a lack of sufficient specimens to perform tests.

According to Eqs. (5)–(7), the BTS and UCS of hard rocks like basalt are the most influential parameters for the performance of a TBM. By reducing either of these parameters, the total performance would be increased. The observed results of this research revealed a significant reduction in BTS and either no reduction or a slight reduction in UCS of the rock samples.

3.5. Temperature distribution in basalt during field simulations

During the field simulations, a small area in the center of the basalt slabs directly in front of the horn antenna was heated by microwave irradiation, indicating that the energy was directed perpendicular to the aperture of the horn waveguide. The diameter of heated area corresponded to the dimension of the aperture of the horn waveguide. The diameter of heated spot on the slab on the top level was approximately 10 cm. The size of the heated area decreased with each successive slab due to the very low thermal conductivity of the rock.

For wet and dry basalt samples exposed to microwaves for 60 s and 120 s at 3 kW power, the closer the rock surface to the aperture of the antenna was, the higher the surface temperature was (Figs. 16–19). A greater distance between the antenna and rock sample allowed the microwaves to bounce off cavity walls, leaving less energy to heat the spot on the rock in front of the antenna. At a given distance, the surface temperature was higher for the 120 s exposure than the 60 s exposure, an effect that was magnified at shorter distances. The temperature decreased exponentially with depth into the sample. The measured penetration depth for dry and wet basalts, was approximately 5 cm, which was in good agreement with the penetration depth calculated from Eq. (1) (4.2 cm).

The surface temperature at approximately 3 cm from the antenna was 20% and 10% higher for the wet samples than that for the

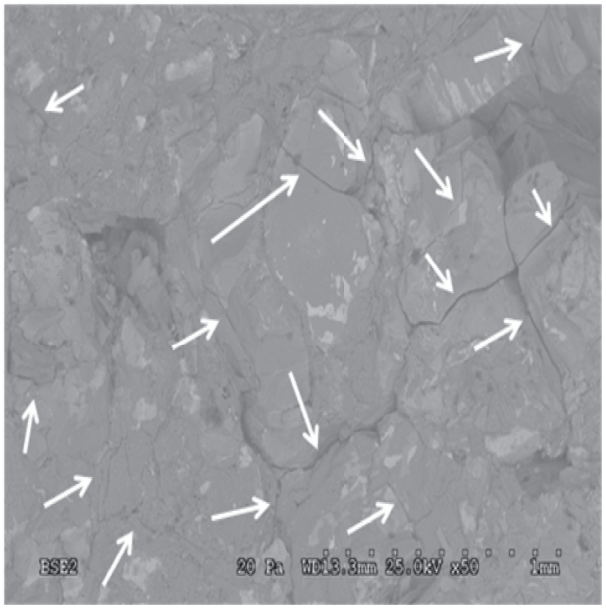

(a)

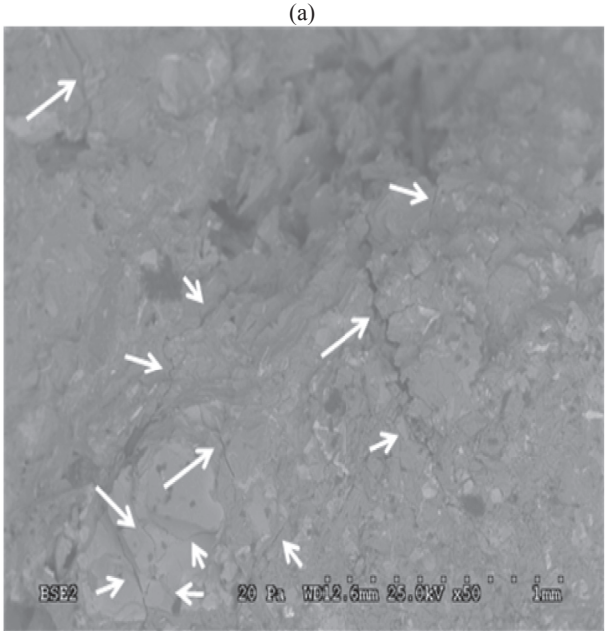

(b)

Fig. 13. Treated (60 s, 3 kW power) basalt #1 SEM images at (a) ×50 and (b) ×200 magnifications.

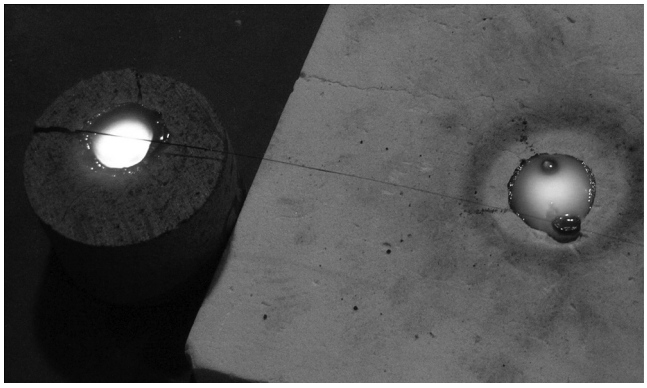

Fig. 14. Basalt #2 disc-shaped specimen melted after microwave treatment for 120 s at 3 kW power.

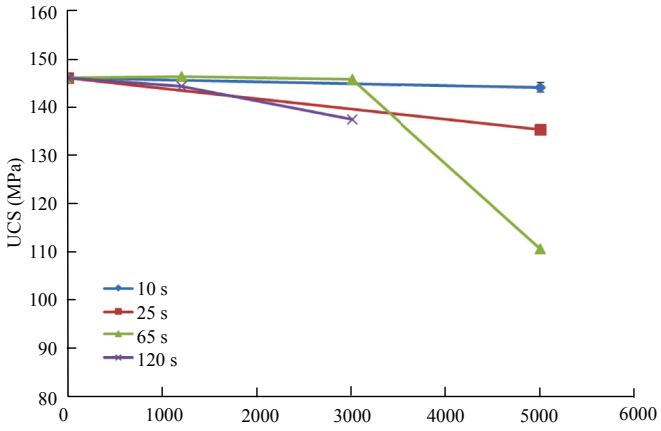

Fig. 15. Basalt #2 UCS vs. microwave power level at four exposure times.

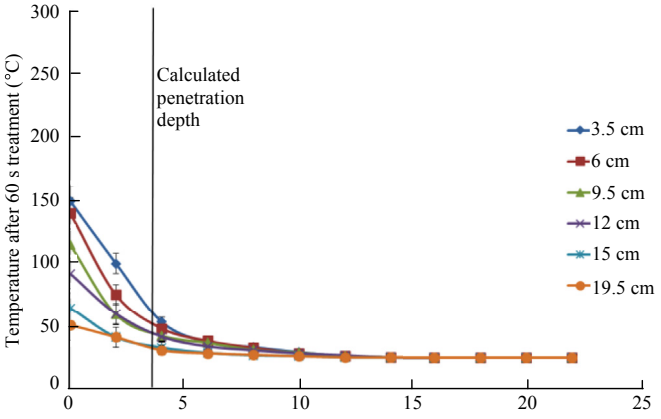

Fig. 16. Measured temperature of dry basalt samples at six distances from the antenna vs. depth along the *z*-axis into the sample after 60 s exposure to microwaves at 3 kW power.

dry samples after 60 s and 120 s exposure, respectively. At longer distances, wet samples were up to 30% cooler than dry samples. This observation can be explained by the thin layer of water on the surface of the topmost slab, which is a strong absorber of microwave energy. The closer the sample to the antenna was, the higher the intensity of microwave energy was and the higher the temperature of the topmost slab was. As the distance between the antenna and rock surface increased, water on the topmost slab absorbed the energy reaching the surface and evaporated, which cooled the rock surface.

The surface temperature of the topmost slab decreased linearly with the distance from the antenna for dry basalts (Fig. 20). The line for the dry basalt radiated for 60 s had a gentler slope than the other three lines. At the 3 cm distance, the temperature difference between dry and wet basalts irradiated for the same time was small, as noted above. However, the difference between the two exposure times was large, with the 120 s exposure yielding temperatures between 250 °C and 300 °C and the 60 s exposure yielding temperatures between 150 °C and 200 °C. Differences among all samples became smaller with increasing distance from the antenna.

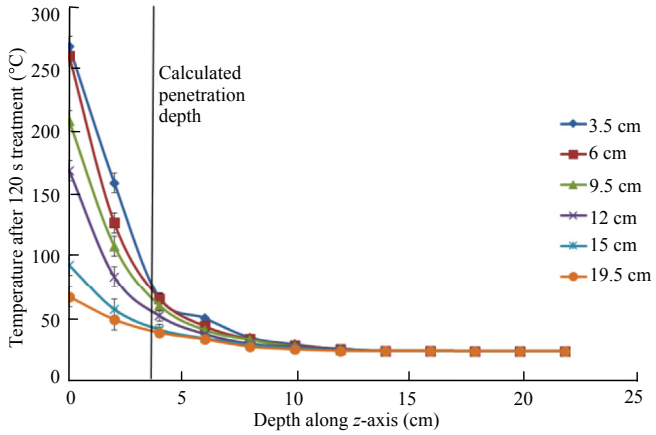

Fig. 17. Measured temperature of dry basalt samples at six distances from the antenna vs. depth along the *z*-axis into the sample after 120 s exposure to microwaves at 3 kW power.

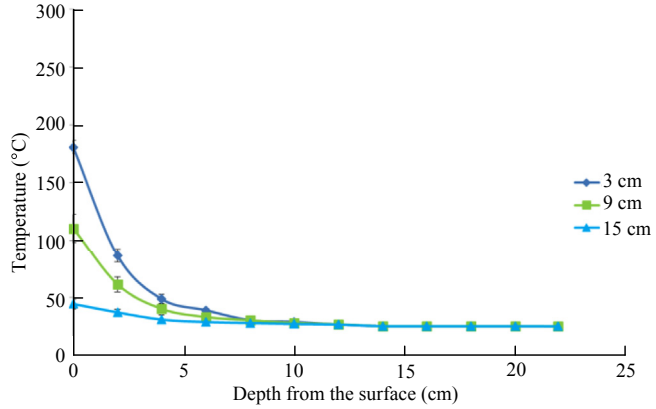

Fig. 18. Temperature of wet basalt samples at three distances from the antenna vs. depth along the *z*-axis into the sample after 60 s exposure to microwaves at 3 kW power.

3.6. Power reflection from basalt during field simulations

For both wet and dry basalts, the amount of energy reflected back to the magnetron from the rock sample was high when the sample was close to the antenna and decreased with distance from the antenna (Fig. 21). With increasing distance between the antenna and rock surface, more space was available for microwaves to bounce between the surface of the rock and the metallic walls of the closed cavity. Therefore, less energy was available to be reflected back to the magnetron.

For dry basalt, the reflected energy attenuated in a sinusoidal form with distance from the antenna (Fig. 21). According to energy propagation theory, the electromagnetic energy from an antenna projected into the free space loses intensity exponentially as the distance from the antenna increases (Eq. (4)). Not all distance points were measured in the wet condition, therefore it is not known if the attenuation line would have shown the same sinusoidal shape as the dry condition. However, it is evident from Fig. 21 that there was less energy reflection overall under wet conditions. This is due to the presence of a very thin layer of water on the top surface of the rock, which absorbs some of the energy emitted and reduces the amount of the microwave energy available for reflection. In other words, adding water to the rock increased the efficiency of the microwave treatment.

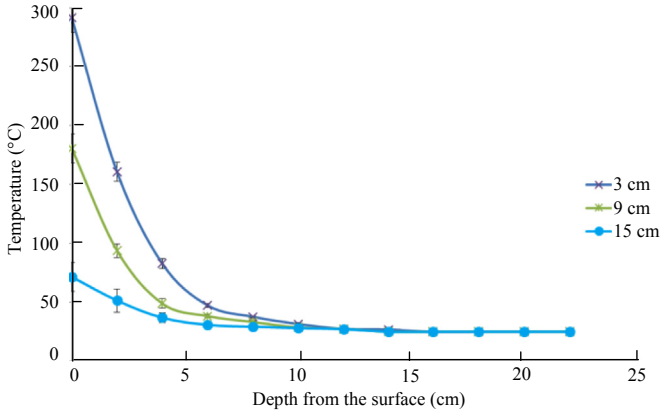

Fig. 19. Temperature of wet basalt samples at three distances from the antenna vs. depth along the *z*-axis into the sample after 120 s exposure to microwaves at 3 kW power.

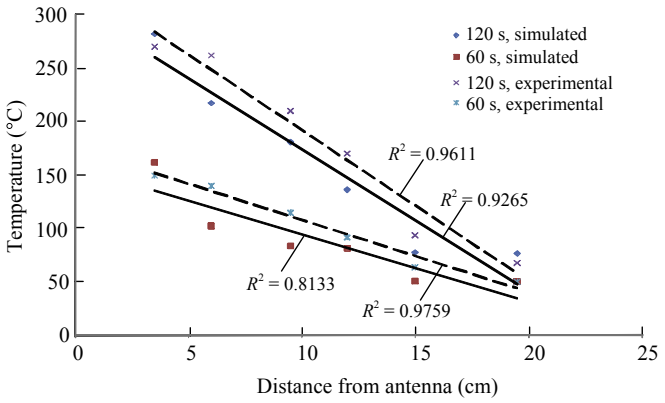

Fig. 20. Experimental (dashed line) and simulated (solid line) mean surface temperatures vs. distance of rock surface from antenna for dry basalts exposed to microwaves for 60 s or 120 s.

3.7. Macro-crack density in basalt after field simulations

The highest macro-crack density in the topmost slab was observed when dry basalt sample was irradiated for 120 s at a

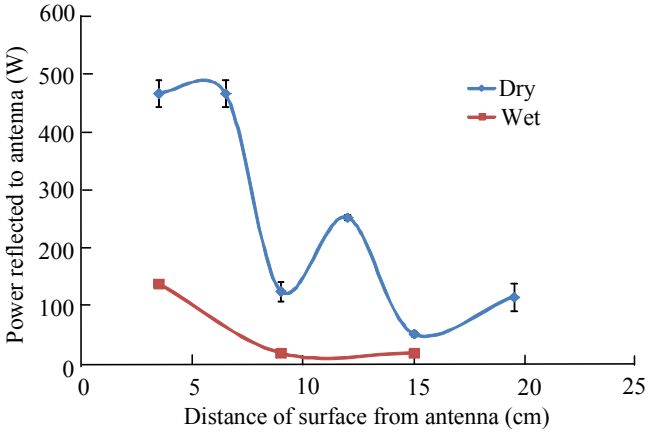

Fig. 21. Reflected power from the surface of the rock to the magnetron at three distances from the antenna.

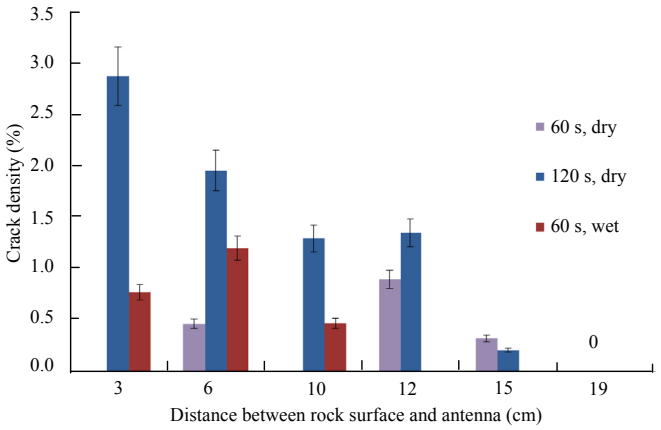

Fig. 22. Mean (±SD) macro-crack density in a 25 cm^2 area on the surface of the topmost slab of wet and dry basalts at various distances from the antenna.

distance of 3 cm from the antenna (Fig. 22). This protocol yielded more macro-cracks than the other two treatments up to a distance of 15 cm. For the 60 s exposure of dry basalt, the most macro-cracks were induced at a distance of 12 cm. Although the dataset is incomplete for wet basalt, it appears that wetting might have increased the ability for the microwaves to induce cracks during 60 s exposure periods, at least at shorter distances.

The distance at which peaks occur (6 cm and 12 cm) fall at 50% and 100% of the wavelength at 2.45 GHz frequency (12.2 cm), where energy intensity is high during microwave propagation through air. This can be observed in Fig. 21 as the power reflection is much higher at half and full wavelength. Although the energy intensity was higher, the overall electric field intensity diminished exponentially as the microwave radiation propagated farther into the material (air and rock). A distance that is less than half of the wavelength is considered a high power intensity zone.

The macro-crack density decreased with each deeper slab, as expected in light of the attenuation of the microwave energy and heat with depth (Fig. 23). The 3 cm and 6 cm distances from the antenna fall in the high power intensity zone; therefore, the macro-crack density is high within the first two slabs, which is in agreement with the penetration rate of microwave calculated theoretically. Longer distances resulted in fewer (or even zero) macro-cracks, even at shallower depth.

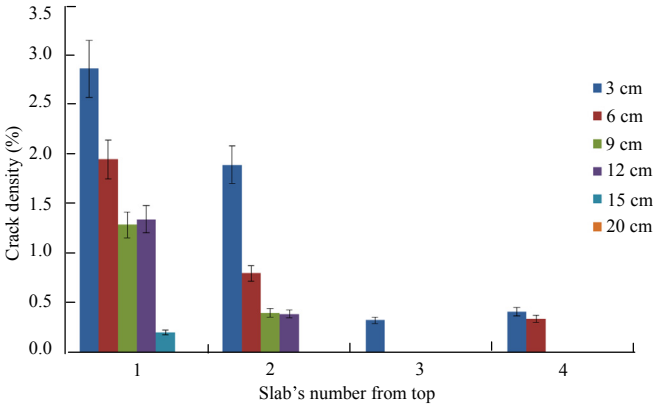

Fig. 23. Mean (±SD) macro-crack density in a 25 cm^2 area on the surface of slabs of dry basalt at various depths.

4. Modeling results and discussion

In the numerical simulations, the exact size of the closed cavity was drawn with a horn antenna inside, as well as a TE01 type of rectangular waveguide connected to the horn antenna (Fig. 24). The rectangular waveguide measures 30 cm long to complete at least one full cycle as the wave travels through the waveguide. Since the wavelength travels a longer distance in waveguides than in air, which is due to phase velocity and cut off frequency of waveguides, the length of waveguide in the simulation is long enough to permit two complete cycles of waves to form within it. The line drawn to the direction of wave propagation in front of the horn antenna is the axis where the energy intensity is collected (Fig. 24).

Two different scenarios were created to validate how microwaves propagate in the cavity. One was an empty cavity and the other contained an absorbent material (the load). The numerical results were compared with the experimental data. In the first scenario (condition), an empty cavity was modeled with all walls to be perfect electrically conductors that completely reflect microwaves (Fig. 25a). This reflection creates a complete chaos of energy inside the cavity, in which the concentration (nodes) of energy changes place repeatedly. However, a pattern was created over time as more energy continuously entered the cavity from the horn antenna.

In the second condition, a block of rock is modeled to be exposed in the microwave cavity and it absorbs the energy according to its ability (Fig. 25b). This absorption changes the microwave propagation pattern. To observe how microwaves propagate when radiated to a large surface, the two sides and bottom were chosen to be in the scattering boundary condition. This allows the walls to behave as normal metallic boundary condition but eliminates the amount of radiation that is reflected from the metal surface. Because there is no reflected radiation bouncing around the cavity, a chaos of energy is not created and straight microwave propagation is observed.

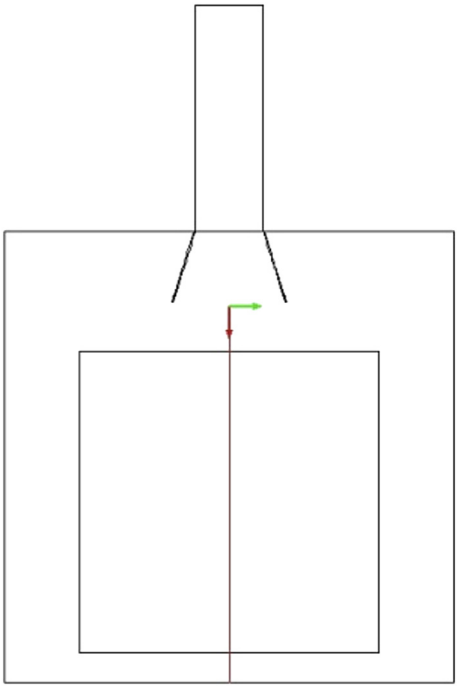

Fig. 24. 2D simulation set up for the microwave closed cavity.

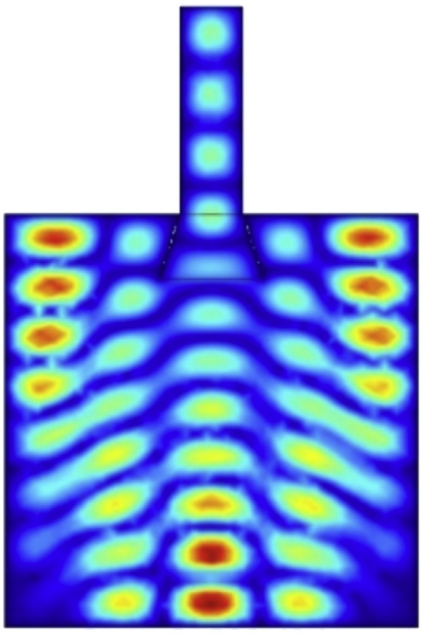

(a)

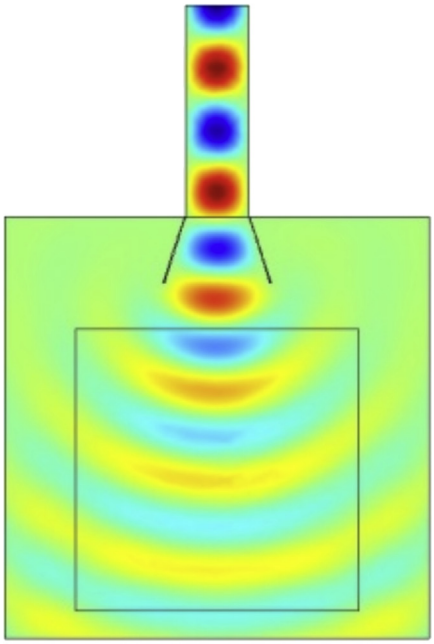

(b)

Fig. 25. Electric field propagation within the closed cavity when walls are (a) perfect electric conductors and (b) in scattering boundary condition (Nekoovaght et al., 2014b).

According to the wave propagation pattern, more energy is emitted in a concentrated area in front of the horn antenna. In other words, there must be a circular area in front of the antenna that absorbs the most energy, which dissipates into heat. The zone that absorbs the most energy within the block of rock exposed to microwave radiation (Fig. 26) is defined by measuring the electromagnetic power loss density within the rock in that zone. Once the radiation energy enters the rock from the surface, where the power loss density is at its maximum (600 W/m^3), the energy intensity exponentially decays. The model computed the maximum power loss density at the surface of basalt sample where it was irradiated by microwaves.

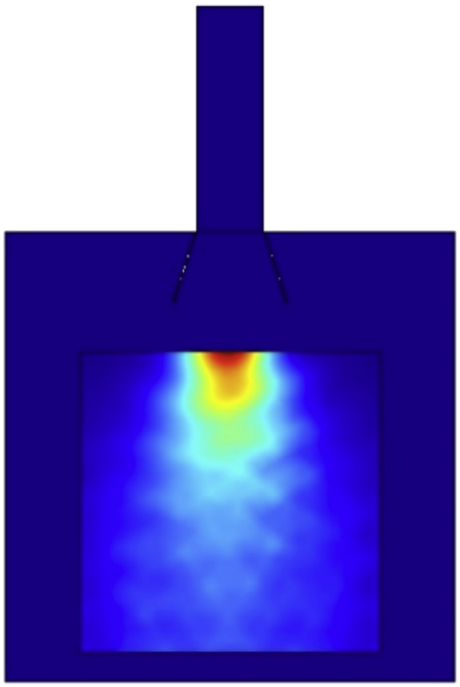

Fig. 26. Electric field energy propagation within the load inside the closed cavity.

4.1. Modeled temperature distribution pattern

The experimental conditions modeled by COMSOL Multiphysics® software include the rectangular and horn waveguides, exposure time, distance to antenna, and cavity dimensions. However, an intact block of rock was the simulated load (Fig. 27), because stacked slabs caused the software to run for days and ultimately crash due to extremely high mesh density in the gaps between slabs.

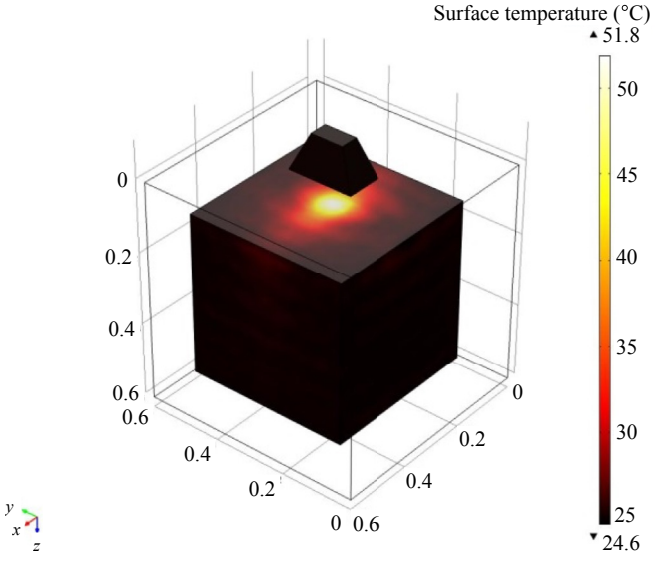

Fig. 27. 3D model of the rock block inside the cavity in front of the horn antenna (Nekoovaght et al., 2014b).

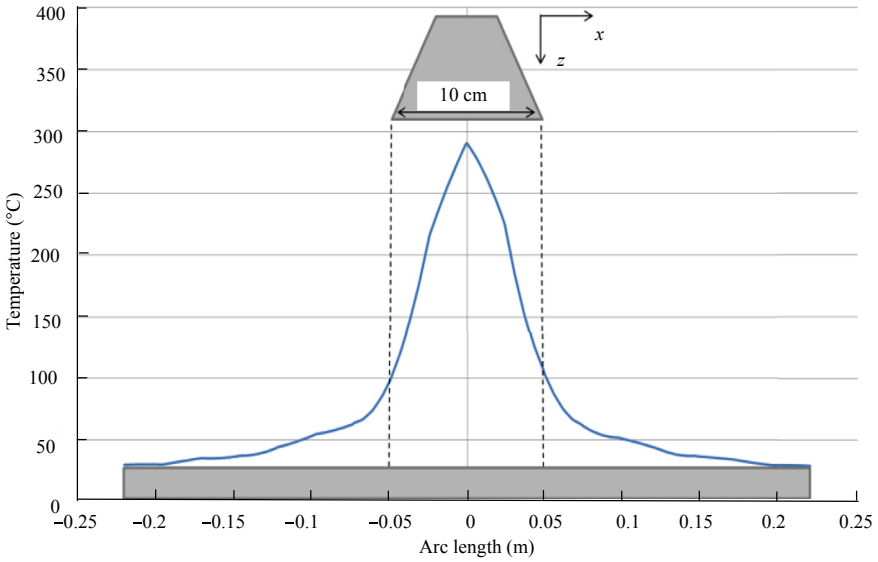

Fig. 28. Modeled temperature distribution along the width of the topmost slab after 60 s of microwave irradiation at 3 kW power from a 10 cm rectangular waveguide.

The modeled topmost slab was exposed to microwave radiation at a distance of 3 cm from the aperture of either a 10 cm (Fig. 28) or 15 cm (Fig. 29) horn waveguide. The temperature distribution demonstrated a rapid rise in temperature in the center of the slab. If 100 °C is considered to be a significantly heated surface, then the area that was significantly heated corresponds to the diameter of the horn waveguide in both models.

The high-temperature zone that was both modeled and observed is in the center of the rock surface in front of the horn antenna. Here, the temperature rose quickly as the exposure time increased (Figs. 28 and 29). In the experiments, when the temperature of the center reached more than 400 °C, chipping initiated in specimens, in the form of very thin bowl-shaped flakes. The maximum diameter of these thin flakes was approximately 5 cm.

The modeled block demonstrated a hot zone exactly in front of the horn antenna, as was observed in experiments (Fig. 27). The temperature distributions along the vertical line illustrated in Fig. 24 correspond well to those observed in the experiments (Figs. 30 and 31). The modeled temperatures at 5 cm depth were slightly higher than that observed ones, due to the uniformity and homogeneity of the rock material. In reality, rock material comprises minerals of differing particle sizes and physical, chemical, and electrical properties, all of which influence the microwave absorption capacity.

The surface temperatures in the models agreed well with experimental data (Fig. 32); the overall trend was that temperature decreases with increasing distance from the horn antenna.

4.2. Microwave power intensity

The temperature decrease with distance from the horn aperture implies a reduction in the power intensity. This phenomenon

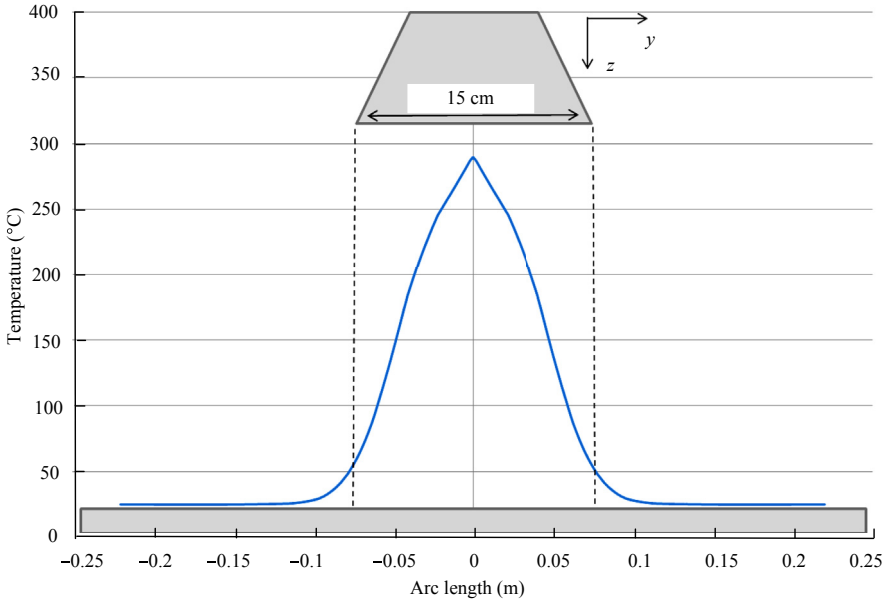

Fig. 29. Modeled temperature distribution along the width of the topmost slab after 60 s of microwave irradiation at 3 kW power from a 15 cm horn waveguide.

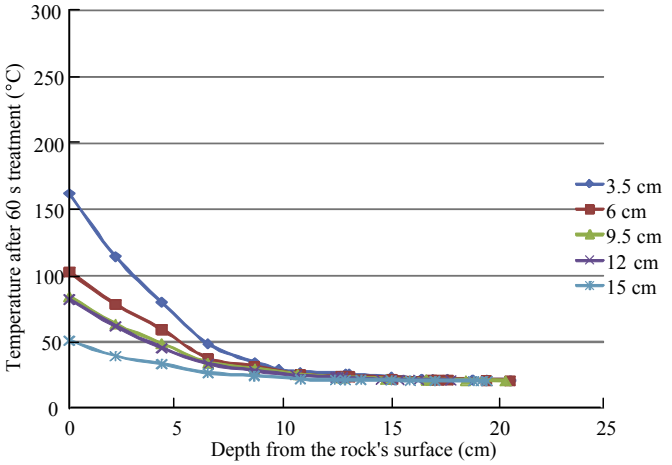

Fig. 30. Simulated temperature of basalt block at five distances from the antenna vs. depth after 60 s exposure to microwaves (Nekoovaght et al., 2014b).

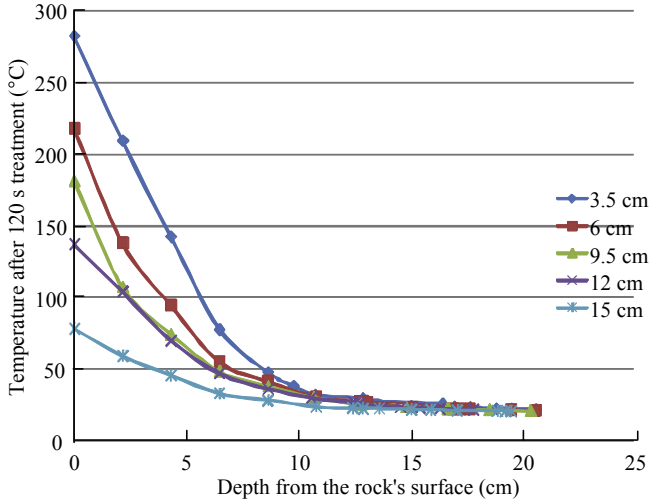

Fig. 31. Simulated temperature of basalt block at five distances from the antenna vs. depth after 120 s exposure to microwaves (Nekoovaght et al., 2014b).

makes sense, since microwave energy dissipates quickly and loses intensity once it exits the waveguide and enters the open air. Although the block of rock was radiated in a closed cavity larger than a standard waveguide (WR340), the microwave energy exited the horn waveguide inside the closed cavity in one direction (perpendicular to the horn antenna aperture). If the rock that absorbs the energy is large and close to the antenna, microwaves do not have enough room to dissipate away from the rock and are absorbed by the rock (Fig. 25). However, as the distance between the antenna and the surface of the load increases, the electric field distribution and microwave propagation within the cavity tend to approach those illustrated in Fig. 25.

According to Eq. (3), the power absorbed and dissipated within a material is directly related to the heating rate of the material. By computing the heating rate of the experimental and modeled blocks of rock at both 60 s and 120 s exposure times, the power intensity reduction can be observed at various distances from the horn antenna aperture. Regardless of the exposure time, the heating rate and power intensity absorbed by the rock decrease with the same linear slope (Fig. 33). Increasing the microwave power increases the heating rate. Imposing a higher heating rate on a

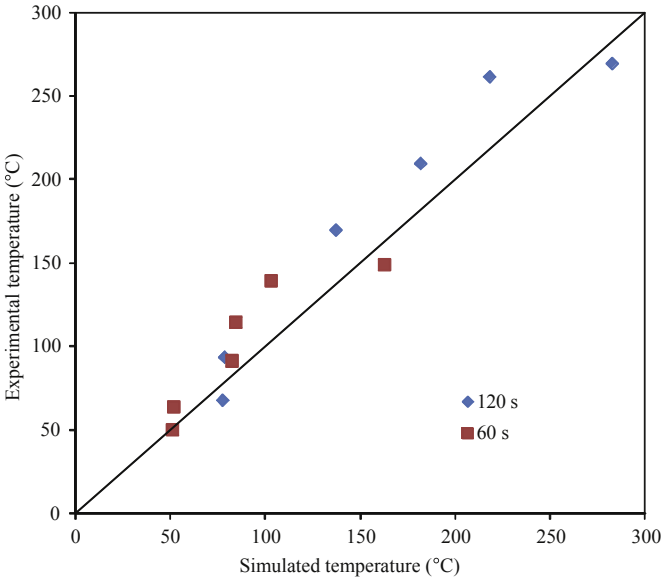

Fig. 32. Measured and simulated surface temperatures.

material with very low thermal conductivity (i.e. rock) generates higher thermal stresses within the material due to differential expansion ratios of particles and quickly induces spalling on the rock surface.

Based upon the direct relationship between the power absorbed and the heating rate in Eq. (3), the linear power reduction observed in Fig. 33 corresponds to the power absorbed from the surface of the irradiated rock at various distances from the horn antenna. However, according to Eq. (4), the power dissipated within the rock is exponentially related to the electric field at various depths. Since the electric field intensity diminishes exponentially within a material, the power absorbed also diminishes exponentially. This trend defines the penetration depth of microwaves into the material.

5. Conclusions and future work

5.1. Conclusions

The susceptibility to microwave treatment varied among the four rock types tested, with norite (obtained using drilling and blasting) being the most susceptible and granite being the least. For

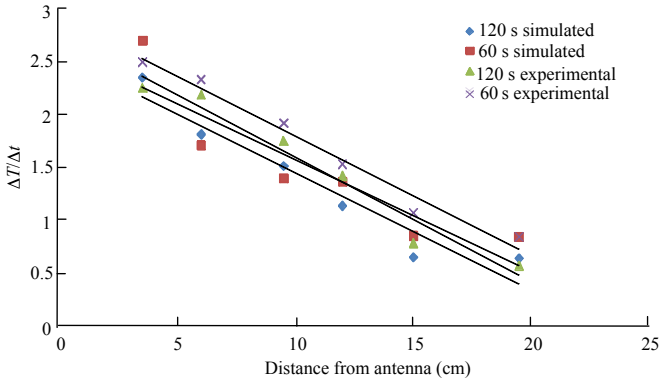

Fig. 33. Measured and modeled rates of temperature change at 3 kW microwave power at various distances from the horn antenna.

a given rock type, the longer the specimen was exposed and the higher the microwave power were, the higher the magnitudes of the BTS and UCS reduction was. The size of the specimen also influenced the heating rate: smaller disc-shaped specimens were heated more rapidly than larger cylindrical samples. The objective was to keep the rocks in the brittle stage to induce physical and mechanical effects within the rock. Therefore, by using a high power level (5 kW), the temperature was increased more quickly and strength reduction occurred with a shorter exposure time.

SEM images of basalt #1 showed that microwave energy induced granular cracks, which reduced the strength of the material and could increase liberation of minerals during processing. Microwave treatment appears to be a very good candidate for use in rock breakage and comminution applications, especially at a high power level. Since microwaves have the ability to penetrate and excite materials from the interior, a combination of microwave preweakening and mechanical rock breakage is proposed.

Field simulations with an open-ended horn waveguide in a closed cavity showed that the influence of water saturation on the temperature gradient in the basalt sample exposed in a microwave field was small, due to the extremely low porosity or water permeability of basalt. Furthermore, higher power intensity was required at a longer distance from the antenna to induce the same damage to the rock surface as a lower power at a shorter distance. Temperature profiles modeled with COMSOL Multiphysics® software agreed well with measured data. This implies that microwaves with higher power intensity are required for rock samples with very low water permeability in order for the energy to cause the very thin layer of water on the surface to evaporate quickly. Rock with higher water permeability would require less microwave energy to undergo mechanical destruction. It is also concluded that microwaves exiting an open-ended waveguide have high power intensity in the vicinity of the antenna, which diminishes exponentially as it travels through a medium (e.g. rock). Therefore, the first half of the wavelength in front of the waveguide can be considered as the high power zone or effective zone.

It is important to note that the microwave-assisted mechanical rock breakage system is feasible and achievable, and in next phase of this project the rock-tool interaction with and without microwave will be evaluated prior to the design of the 1st prototype system.

5.2. Future work

The high performance computing resources of the McGill HPC system under Compute Canada together with COMSOL, ANSYS and EDEM softwares will be used for this purpose. The model will be calibrated and validated against experimental data. An improved understanding on the mechanism of wave penetration, temperature profiles and rock stress (damages and cracks) can be achieved by taking into account variation in rock properties, inhomogeneity and pre-existing discontinuities. A parametric study and optimization will be carried out to arrive at the best design and operating parameters. Discrete element modeling for thermally induced rock damage is a natural choice and referred to in the future work. The reason that it was ruled out by the authors is that no commercial discrete element software is available today to correlate thermal stress to bond breakage between particles. However, from the employment of continuum based model, the temperature field can be determined and the thermal gradient can be correlated to thermal stress and micro-cracks density. For the future work, however, the authors plan to use the thermal stress determined from a finite element based model and then feed it into discrete element software as a force field to compare the micro-crack density.

Conflict of interest

We wish to confirm that there are no known conflicts of interest associated with this publication and there has been no significant financial support for this work that could have influenced its outcome.

Acknowledgments

It is a pleasure to acknowledge the Natural Sciences and Engineering Research Council of Canada (NSERC) with the collaboration of IAMGold, Glencore, and Vale Canada, who generously contributed financially to this research project. Special thanks to Dr. Marc Bétournay from Natural Resources Canada (CANMET) for his advice, help and encouragement. Thanks to all the members of GeoMechanics team.

References

ASTM International. ASTM 70122−04, Standard test method for compressive strength and elastic moduli of intact rock core specimens under varying states of stress and temperatures. West Conshohocken, PA: ASTM International; 2004. http://dx.doi.org/10.1520/D7012-04.

ASTM International. ASTM 39677−05, Standard test method for splitting tensile strength of intact rock core specimens. West Conshohocken, PA: ASTM International; 2005. http://dx.doi.org/10.1520/D3967-05.

Brodie G. Microwave heating in moist materials. In: Grundas S, editor. Advances in induction and microwave heating of mineral and organic materials. InTech; 2011. p. 553−84. http://dx.doi.org/10.5772/13422.

Carmichael RS. Practical handbook of physical properties of rocks and minerals. Boca Raton, FL: CRC Press; 1988.

Chen TT, Dutrizac JE, Haque KE, Wyslouzil W, Kashyap S. The relative transparency of minerals to microwave radiation. Canadian Metallurgical Quarterly 1984;23(3):349−51.

Fitzgibbon KE, Veasey TJ. Thermally assisted liberation—a review. Minerals Engineering 1990;3(1−2):181−5.

Gray W. Surface spalling by thermal stresses in rock. In: Proceedings of the Rock Mechanics Symposium. Ottawa, ON, Canada: Mines Branch Dept. Mines and Technical Surveys; 1965. p. 85−106.

Griffiths DJ. Introduction to electrodynamics. 3rd ed. Upper Saddle River, NJ: Prentice Hall; 1999.

Gwarek W, Celuch-Marcysiak M. A review of microwave power applications in industry and research. In: The 15th International Conference on Microwaves, Radar and Wireless Communications (MIKON-2004). IEEE; 2004. p. 843−8.

Harrison PC. A fundamental study of the heating effect of 2.45 GHz microwave radiation on minerals. PhD Thesis. Birmingham: Chemical Engineering Department, Birmingham University; 1997.

Hassani F. Review of explosive-free rock breakage (EFRB) technologies. Montreal, Canada: McGill University; 2010.

Hassani F, Nekoovaght P. The development of microwave assisted machineries to break hard rocks. In: Proceedings of the 28th International Symposium on Automation and Robotics in Construction (ISARC). Seoul: South Korea; 2011. p. 678−84.

Hassani F, Nekoovaght P. The use of microwave to contribute to breakage of rocks. In: The 2nd South American Symposium on Rock Excavations, San José, Costa Rica; 2012.

Hassani F, Nekoovaght PM, Radziszewski P, Waters KE. Microwave assisted mechanical rock breaking and application. In: Canadian Institute of Mining and Materials (CIM) Conference and Exhibition, Montreal, Canada; 2011.

Hassani F, Nekoovaght PM, Radziszewski P, Waters KE. Microwave assisted mechanical rock breaking. In: Harmonising Rock Engineering and the Environment—Proceedings of the 12th ISRM International Congress on Rock Mechanics. Beijing: CRC Press; 2012. p. 2075−80.

Hassani F, Ouellet J, Radziszewski P, Nokken M, Nekoovaght P. Microwave assisted drilling and its influence on rock breakage. In: The 5th Asian Rock Mechanics Symposium (ARMS 2008), Vol. 1. ISRM; 2008. p. 87−104.

Hoek E, Bieniawski ZT. Brittle fracture propagation in rock under compression. International Journal of Fracture 1965;1(3):137−55.

Kingman SW, Rowson NA. Microwave treatment of minerals—a review. Minerals Engineering 1998;11(11):1081−7.

Kingman SW, Corfield GM, Rowson NA. Effects of microwave radiation upon the mineralogy and magnetic processing of a massive Norwegian ilmenite ore. Magnetic and Electrical Separation 1998;9(3):131−48.

Kingman SW, Jackson K, Bradshaw SM, Rowson NA, Greenwood R. An investigation into the influence of microwave treatment on mineral ore comminution. Powder Technology 2004;146(3):176−84.

Lauriello PJ, Fritsch CA. Design and economic constraints of thermal rock weakening techniques. International Journal of Rock Mechanics and Mining Sciences & Geomechanics Abstracts 1974;11(1):81−9.

Maurer W. Novel drilling techniques. London: Pergamon Press; 1968.
Meredith RJ. Engineers' handbook of industrial microwave heating. London, UK: Institution of Electrical Engineers; 1998.
Metaxas AC, Meredith RJ. Industrial microwave heating. London: Peter Peregrinus Ltd.; 1983.
Nekoovaght P, Hassani F. The influence of microwave radiation on hard rocks as in microwave assisted rock breakage applications. In: Rock Engineering and Rock Mechanics: Structures in and on Rock Masses, the ISRM European Rock Mechanics Symposium (EUROCK 2014). Vigo, Spain; 2014. p. 195–8.
Nekoovaght P, Gharib N, Hassani F. Numerical simulation and experimental investigation of the influence of microwave radiation on hard rock surface. In: Rock Mechanics for Global Issues–Natural Disasters, Environment and Energy, the 8th Asian Rock Mechanics Symposium (ARMS8). Sapporo, Japan; 2014.
Nekoovaght P, Gharib N, Hassani F. Microwave assisted rock breakage for space mining. In: ASCE's Aerospace Division, the 14th Earth and Space Conference. St. Louis, USA; 2014.
Nekoovaght P, Gharib N, Hassani F. Microwave assistance positive influence on rock breakage in space mining applications. In: The 65th International Astronautical Congress. Toronto, Canada; 2014.
Nekoovaght P, Gharib N, Hassani F. The behavior of rocks when exposed to microwave radiation. In: The 13th International Congress on Rock Mechanics (ISRM). Montreal, Canada; 2015.
Osepchuk JM. A history of microwave heating applications. IEEE Transactions on Microwave Theory and Techniques 1984;32(9):1200–24.
Resource Technology Inc. A technical and economical evaluation of thermal spallation drilling technology. Tulsa, Oklahoma: Resource Technology Inc.; 1984.
Saxena AK. Electromagnetic theory and applications. Oxford, UK: Alpha Science International; 2009.
Schön JH. Physical properties of rocks: fundamentals and principles of petrophysics. Amsterdam, Oxford: Elsevier; 2004.
Scott G. Microwave pre-treatment of a low grade copper ore to enhance milling performance and liberation. Stellenbosch, South Africa: Department of Process Engineering, University of Stellenbosch; 2006. MS Thesis.
Walkiewicz JW, Clark AE, McGill SL. Microwave-assisted grinding. IEEE Transactions on Industry Applications 1991;27(2):239–43.
Wang G, Radziszewski P, Ouellet J. Exploring DEM model development for the simulation of thermal effects on ore breakage. Montreal, Canada: Department of Mining and Materials Engineering, McGill University; 2005.
Whittle DN, Kingman SW, Reddish DJ. Application of numerical modelling for prediction of the influence of power density on microwave-assisted breakage. International Journal of Mineral Processing 2003;68(1–4):71–91.
Wijk G. A model of tunnel boring machine performance. Geotechnical and Geological Engineering 1992;10(1):19–40.
Wilkinson MA, Tester JW. Experimental measurement of surface temperatures during flame-jet induced thermal spallation. Rock Mechanics and Rock Engineering 1993;26(1):29–62.

Ferri Hassani obtained his Bachelor of Mining Engineering and Ph.D. from Nottingham University, Nottingham England in 1976 and 1981, respectively. Ferri Hassani is a Webster Chair Professor of Mining Engineering at McGill University and director of Geo-mechanics labs and Earth/Mine Energy Research Group (EMERG), England. He was awarded a Fellow of the Canadian Institute of Mining and Metallurgy for his contribution to the mining industry in Canada. He has been at McGill University since 1983 and many years in a leadership role. His focus evolved from rock mechanics and mine design, to mining and energy and waste heat recovery from mining operation mine waste disposal, minefill and mining sustainability as well as microwave assisted rock breaking system. He was one of the pioneers of Pate backfill and he is the chairman of the International Mine Backfill Council. He was Co-founder and Chairman of the Canadian Mining Innovation Council (CMIC). He was given Canadian Rock Mechanics Award of Rock Engineering Society of CIM in 1992 and was also awarded Boleslaw Krupinski Gold Medal from the World Mining Organization of IOC 2013. He continues to maintain a strong interdisciplinary research and consulting activities with several million dollars of research and has graduated over 150 Ph.D. and MEng. Students, as well as research assistants, post-doctoral fellows, research associates and published over 160 scientific articles and reports. His research has led to obtaining several patents in the past 15 years.